



Design, analysis and validation of the bridge-type displacement amplification mechanism with circular-axis leaf-type flexure hinges for micro-grasping system

Weilin Chen¹ · Qinghua Lu¹ · Chuiwang Kong¹ · Yunzhi Zhang¹ · Qinghua Zhang¹

Received: 20 May 2018 / Accepted: 20 July 2018 / Published online: 9 August 2018
© Springer-Verlag GmbH Germany, part of Springer Nature 2018

Abstract

For stable and flexible manipulation, realizing parallel grasping and large output stroke simultaneously has become a key issue in the researches on micro-grasping system. The typical solution is to use compliant orthogonal displacement amplification mechanism (such as bridge-type mechanism), in which the flexure hinges are generally axial load-dominated, whereas the deflection of traditional straight-axis flexure hinges is not related to the axial load under small deflection assumption. In this study, a bridge-type mechanism with circular-axis leaf-type (CALT) flexure hinges is designed, analyzed and validated. Through modeling the generalized displacements of CALT flexure hinge, the positive direction of its axis in the bridge-type mechanism is designed. The precise models of load relations for the CALT flexure hinges in the bridge-type DAM are established, and the multi-objective parametric optimization is further given. Small deflection-based static FEA results verify the generalized displacements' models of CALT flexure hinge as well as the parametric optimization result. Compared with the corresponding bridge-type mechanism with the largest output displacement in the traditional researches, the output displacement of optimal result is improved effectively. For the design validation, the optimal design result is further applied to construct a piezoelectric-driven microgripper, which grasps parallelly and enlarges the output stroke simultaneously.

1 Introduction

Micro-grasping system focuses on the grasping of objects ranging from several hundred nanometers to several hundred micrometers, which is widely applied in cell manipulation (Liu et al. 2017b), optic fiber assembly (Chen et al. 2013) and microsystem components testing (Piriyanont et al. 2015). For the stable and flexible manipulation, realizing parallel grasping and large output stroke simultaneously has become a key issue in the researches on micro-grasping system.

One idea is to utilize the orthogonal displacement amplification mechanism (DAM), including single-stage type and multi-stage type. Without clearance, backlash and friction, compliant mechanisms are widely used to construct micro-grasping systems (Howell 2001). Bridge-type

mechanism is a typical single-stage compliant orthogonal DAM (Pokines and Garcia 1998), for which the actuator can be placed inside the mechanism and the displacement amplification ratio is not related to the length of beam. Lobontiu and Garcia modeled and optimized the bridge-type mechanism with straight-axis flexure hinges in terms of kinematics and statics (Lobontiu and Garcia 2003). Kim et al. (2003) proposed a three dimensional bridge-type mechanism. Mottard and Stamant (2009) analyzed the orientation of straight-axis flexure hinges in bridge-type DAM, finding out that the maximal stress significantly decreased when the flexure hinges incline. Xu and Li (2011) analytically modeled, optimized and tested the compound bridge-type mechanism. Kim et al. (2012) proposed a double-compound bridge-type mechanism. Both the compound bridge-type mechanism and the double-compound bridge-type mechanism can improve the lateral stiffness at the output ports. Ham et al. (2016) tested the kinetic response of bridge-type mechanism. Wei et al. (2017) established the general static models describing the bridge-type mechanism with leaf-type flexure hinges as well as Rhombic bridge-type mechanism. Dong et al.

✉ Qinghua Lu
qhlu@fosu.edu.cn

¹ School of Mechatronics Engineering, Foshan University, Foshan 528000, China

(2017) designed a high-efficient bridge-type mechanism based on negative stiffness. Further, Chen et al. (2017a, b) proposed and optimized a novel compliant orthogonal DAM which reserved the advantage of bridge-type mechanism without requiring bidirectional symmetric input forces. The general principle of multi-stages compliant orthogonal DAM is to combine one or several single-stage DAMs (such as leverage mechanism, and bridge-type mechanism) with compliant parallelogram (Xing 2015; Sun et al. 2015), for which the design constraints are simple whereas it occupies considerable space compared with the single-stage orthogonal DAM.

Most of the compliant orthogonal DAMs are flexure-based. Flexure hinges can be divided into two classifications, the straight-axis type (Chen 2014; Liu et al. 2017a) and the curve-axis type (Wang et al. 2015; Kozuka et al. 2013; Lobontiu and Cullin 2013; Verotti et al. 2015). The researches on straight-axis flexure hinges are sufficient, and leaf-type flexure hinge is considered as the straight-axis one with the largest compliance along the deflection direction. Most of the traditional researches focus on the design, analysis and test of bridge-type mechanisms with straight-axis flexure hinges. Generally, the flexure hinges in bridge-type mechanisms are axial force-dominated, whereas the deflection of straight-axis flexure hinge is not related to the axial load under small deflection assumption (Yong et al. 2008; Lin et al. 2013). Bridge-type mechanisms have fully symmetric structure, which can eliminate the problem that curve-axis flexure hinges lead to designs with low stiffness along the undesired motion directions (Ma and Chen 2015).

Different from the traditional researches, this paper focuses on the design, analysis and validation of bridge-type mechanism with circular-axis leaf-type (CALT) flexure hinges, which vary from typical straight-axis flexure hinges to typical curve-axis flexure hinges with the change of radius angles. In Sect. 2, through modeling the generalized displacements of CALT flexure hinge, the positive direction of its axis in the bridge-type mechanism will be designed. In Sect. 3, the relation among the loads act on each CALT flexure hinge in the bridge-type mechanism will be established. In Sect. 4, the parameters of CALT flexure hinges in the bridge-type mechanism will be optimized. In Sect. 5, the static models of CALT flexure hinges as well as the optimal results will be verified by finite element analysis (FEA). Further, the optimal design results will be applied to construct a piezo-driven microgripper for the design validation.

2 Structural design of the bridge-type DAM with CALT flexure hinge

2.1 Step 1: static modeling of the CALT flexure hinge

CALT flexure hinge is illustrated in Fig. 1a. Arcs AD, BC are named as the inner arc and the outer arc respectively. The positive direction of axis is hence from the outer arc towards the inner arc. Figure 1b shows the force analysis, in which the width along Z axis is a constant b . When $\theta_h \rightarrow 0$, leaf-type flexure hinge, a typical straight-axis flexure hinge, is obtained, as shown in Fig. 1c. When $\theta_h \rightarrow \pi$, the bio-inspired flexure hinge shown in Kozuka et al. (2013), which is a typical curve-axis flexure hinge, is obtained, as shown in Fig. 1d.

For constant cross-sectional cantilever ABCD, loads F_{xs} , F_{ys} , M_s are exerted at end s. The force F_{ys} is along AD, which is named as the “nominal axis”. The force F_{xs} is perpendicular to AD, and the corresponding displacement is named as the “nominal deflection”. Under small deflection assumption (for example, the deflection of point s is smaller than $0.1t$), the generalized displacement-load relation at point s can be described by Castigliano’s second theorem:

$$x_s = \frac{\partial V_{ABCD}}{\partial F_{xs}}, \quad \theta_s = \frac{\partial V_{ABCD}}{\partial M_s}. \quad (1)$$

If cantilever ABCD is an Euler-Bernoulli beam, for which the shear effect can be ignored. The strain energy V_{ABCD} thereby consists of the axial and the bending deformation terms:

$$V_{ABCD} = \int_0^L \frac{F_a^2}{2EA} dp + \int_0^L \frac{M^2}{2EI} dp, \quad (2)$$

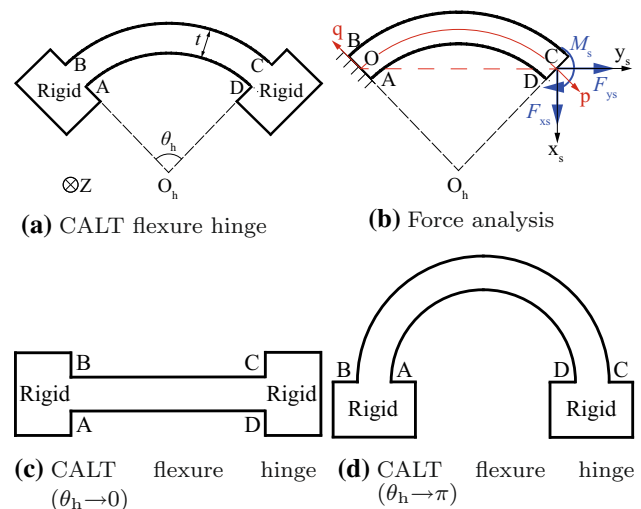


Fig. 1 CALT flexure hinge

where L denotes the length of beam ABCD, and E denotes the Young’s Modulus. The cross-sectional area $A = b t$, and the cross-sectional moment of inertia $I = \frac{bt^3}{12}$. The axial force F_a and the bending moment M are formulated as:

$$F_a = F_{ys} \cos\left(\frac{\theta_h}{2} - \frac{p\theta_h}{L}\right) - F_{xs} \sin\left(\frac{\theta_h}{2} - \frac{p\theta_h}{L}\right). \tag{3}$$

$$M = \frac{L}{\theta_h} \left[\cos\left(\frac{\theta_h}{2} - \frac{p\theta_h}{L}\right) - \cos\frac{\theta_h}{2} \right] F_{ys} - \frac{L}{\theta_h} \left[\sin\left(\frac{\theta_h}{2} - \frac{p\theta_h}{L}\right) + \sin\frac{\theta_h}{2} \right] F_{xs} - M_s. \tag{4}$$

Equations (1)–(4) lead to that:

$$x_s = \int_0^L \left(\frac{mn}{EA} + \frac{uv}{EI} \right) dp \cdot F_{ys} + \int_0^L \left(\frac{n^2}{EA} + \frac{v^2}{EI} \right) dp \cdot F_{xs} + \left(- \int_0^L \frac{v}{EI} dp \right) \cdot M_s, \tag{5}$$

$$\theta_s = - \frac{1}{EI} \int_0^L u dp \cdot F_{ys} - \frac{1}{EI} \int_0^L v dp \cdot F_{xs} + \frac{L}{EI} M_s, \tag{6}$$

where the parameters m, n, u, v are:

$$\begin{aligned} m &= \cos\left(\frac{\theta_h}{2} - \frac{p\theta_h}{L}\right), \quad n = -\sin\left(\frac{\theta_h}{2} - \frac{p\theta_h}{L}\right), \\ u &= \frac{L}{\theta_h} \left[\cos\left(\frac{\theta_h}{2} - \frac{p\theta_h}{L}\right) - \cos\frac{\theta_h}{2} \right], \\ v &= - \frac{L}{\theta_h} \left[\sin\left(\frac{\theta_h}{2} - \frac{p\theta_h}{L}\right) + \sin\frac{\theta_h}{2} \right]. \end{aligned} \tag{7}$$

2.2 Step2: designing the positive direction of axes for the CALT flexure hinges in the bridge-type DAM

In bridge-type DAM, all the flexure hinges are nominal axial elongation force-dominated. Therefore, if the CALT flexure hinges shown in Fig. 1 are applied in bridge-type mechanism, F_{ys} is dominated compared with F_{xs} as well as M_s , and F_{ys} is positive. In this situation, Eq. (5) is simplified as:

$$\begin{aligned} x_s &\approx \int_0^L \left(\frac{mn}{EA} + \frac{uv}{EI} \right) dp \cdot F_{ys} \\ &= \left(\frac{1}{EA} \int_0^L mndp + \frac{1}{EI} \int_0^L uvdp \right) \cdot F_{ys}. \end{aligned} \tag{8}$$

According to Eq. (7) and the trigonometric identities,

$$\begin{aligned} \int_0^L mndp &= 0, \\ \int_0^L uvdp &= - \left(\frac{L}{\theta_h} \right)^2 \left[\frac{L}{\theta_h} (1 - \cos\theta_h) - \frac{1}{2} \sin\theta_h \cdot L \right], \end{aligned} \tag{9}$$

where $(\frac{1}{2} \sin\theta_h \cdot L) / [\frac{L}{\theta_h}(1 - \cos\theta_h)] = \frac{\theta_h}{2} / \tan\frac{\theta_h}{2}$. Since the range of θ_h is $(0, \pi)$, $\frac{\theta_h}{2} / \tan\frac{\theta_h}{2}$ is smaller than 1. Thus, the coefficient of Eq. (8) is negative. Further considering $F_{ys} > 0$, x_s is hence negative, which indicates that the free end of CALT flexure hinge deflects along the negative direction of its axis when the elongation forces are applied along the nominal axis. Therefore, if the bridge-type DAM with the CALT flexure hinges is designed as Fig. 2, the grasping output movement can be further enlarged.

3 Precise model of the load relations for the CALT flexure hinges in the bridge-type DAM

In Fig. 2, the boundary conditions of beam 1–2–3–4 is $Y_4 = 0, \theta_4 = 0, X_1 = 0, \theta_1 = 0$. The mechanism is symmetric to the input force F_{in} and output axis mn simultaneously. Furthermore, F_{in} is symmetric to output axis mn. Therefore, the force analysis of beam 1–2–3–4 is shown in Fig. 3a, where $F_{y1} = \frac{1}{2} F_{in}$. According to the load equilibrium of beam 1–2–3–4,

$$F_{y1} = F_{y4}, \quad M_4 - M_1 + F_{y1}t_r = 0. \tag{10}$$

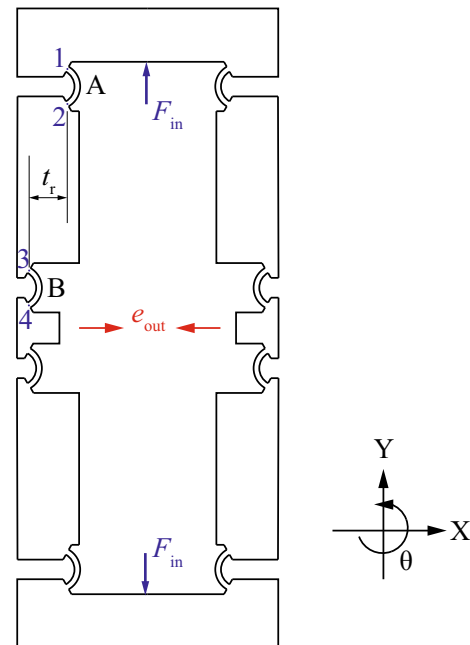


Fig. 2 Bridge-type DAM with CALT flexure hinges

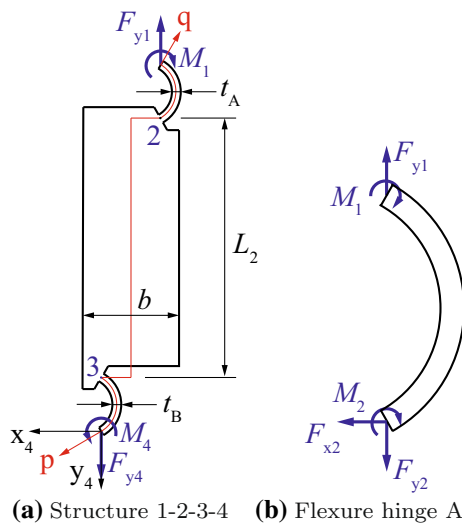


Fig. 3 Force analysis of structure 1–2–3–4 and the flexure hinge A

Assume that beam 1–2–3–4 is satisfied with small deflection assumption. When point 1 is chosen as the origin, θ_4 can be formulated by Castigliano’s Second Theorem as:

$$\theta_4 = \frac{\partial V_\varepsilon}{\partial M_4}. \tag{11}$$

If structure 1–2–3–4 is an Euler–Bernoulli beam, the shear effect can be ignored. Thus, the strain energy V_ε is:

$$V_\varepsilon = \int_0^{L_p} \frac{F_{ap}^2}{2EA_p} dp + \int_0^{L_p} \frac{M_{ap}^2}{2EI_p} dp, \tag{12}$$

where $L_p = l_A + L_2 + l_B$. The parameters l_A, l_B denote the length of flexure hinges A, B respectively. In Eq. (12), the axial force F_{ap} is not related to M_4 , and the bending moment M_{ap} is formulated as:

$$M_{ap} = \begin{cases} \left\{ \frac{l_A}{\theta_{hA}} \left[\cos \left(\frac{p\theta_{hA}}{l_A} - \frac{\theta_{hA}}{2} \right) - \cos \frac{\theta_{hA}}{2} \right] + t_r \right\} F_{y4} + M_4 & (0 < p < l_A) \\ \frac{t_r}{2} F_{y4} + M_4 & (l_A < p < l_A + L_2) \\ \left\{ \frac{l_B}{\theta_{hB}} \left[\cos \left(\frac{(p - l_A - L_2)\theta_{hB}}{l_B} - \frac{\theta_{hB}}{2} \right) - \cos \frac{\theta_{hB}}{2} \right] \right\} F_{y4} + M_4 & (l_A + L_2 < p < l_A + L_2 + l_B) \end{cases} \tag{13}$$

where θ_{hA} and θ_{hB} are the radius angles of flexure hinges A, B respectively. With the combination of Eqs. (11)–(13) as well as $\theta_4 = 0$, the relation between F_{y4} and M_4 is obtained as:

$$\eta F_{y4} + \Omega M_4 = 0, \tag{14}$$

where the coefficients η and Ω are:

$$\eta = \frac{1}{E \frac{ht_A^3}{12}} eta1 + \frac{\frac{t_r}{2}}{E \frac{hb^3}{12}} L_2 + \frac{1}{E \frac{ht_B^3}{12}} eta2, \tag{15}$$

$$\Omega = \frac{1}{E \frac{ht_A^3}{12}} l_A + \frac{1}{E \frac{hb^3}{12}} L_2 + \frac{1}{E \frac{ht_B^3}{12}} l_B.$$

In Eq. (15), $eta1$ and $eta2$ are two integrals, as shown in Eq. (16).

$$eta1 = \int_0^{l_A} \left\{ \frac{l_A}{\theta_{hA}} \left[\cos \left(\frac{p\theta_{hA}}{l_A} - \frac{\theta_{hA}}{2} \right) - \cos \frac{\theta_{hA}}{2} \right] + t_r \right\} dp$$

$$eta2 = \int_{l_A+L_2}^{L_p} \frac{l_B}{\theta_{hB}} \left[\cos \left(\frac{p - l_A - L_2}{l_B} \theta_{hB} - \frac{\theta_{hB}}{2} \right) - \cos \frac{\theta_{hB}}{2} \right] dp \tag{16}$$

According to Eqs. (10) and (14), the relationship between F_{y1} and M_1 is obtained as:

$$M_1 = F_{y1} \left(t_r - \frac{\eta}{\Omega} \right). \tag{17}$$

The force analysis of flexure hinge A is shown in Fig. 3b, and the load equilibrium equations are:

$$F_{x2} = 0, \quad F_{y2} = F_{y1}, \quad M_2 = -M_1. \tag{18}$$

4 Parametric optimization of the CALT flexure hinges in the bridge-type DAM

Applying Eqs. (5) and (6) to point 2 in the flexure hinge A and considering the load relation (Eqs. 17, 18) as well as $F_{y1} = \frac{1}{2} F_{in}$, the nominal deflection and the rotation at point 2 are formulated as:

$$\begin{aligned}
 x_2 &= \left[\int_0^{l_A} \left(\frac{mn}{EA_A} + \frac{uv}{EI_A} \right) dp + \int_0^{l_A} \frac{v}{EI} dp \cdot \left(t_r - \frac{\eta}{\Omega} \right) \right] \cdot \frac{1}{2} F_{in}, \\
 \theta_2 &= \left[-\frac{1}{EI_A} \int_0^{l_A} u dp - \frac{l_A}{EI_A} \left(t_r - \frac{\eta}{\Omega} \right) \right] \frac{1}{2} F_{in}.
 \end{aligned}
 \tag{19}$$

Assuming that the linkage between A and B is a rigid body, the displacement x_3 is calculated by the geometrical relation as:

$$|x_3| = t_r - \left[\sqrt{t_r^2 + L_2^2} \cdot \sin \left(\arcsin \frac{t_r}{\sqrt{t_r^2 + L_2^2}} - |\theta_2| \right) - |x_2| \right].
 \tag{20}$$

Applying Eq. (5) to point 4 in the flexure hinge B and considering the load relation (Eqs. 10, 14) as well as $F_{y1} = \frac{1}{2} F_{in}$, the nominal deflection at point 4 due to elastic deformation are formulated as:

$$x_{4e} = \left[\int_0^{l_B} \left(\frac{mn}{EA_B} + \frac{uv}{EI_B} \right) dp - \int_0^{l_B} \frac{v}{EI} dp \cdot \frac{\eta}{\Omega} \right] \frac{1}{2} F_{in}.
 \tag{21}$$

Since $x_2 < 0$ and $x_{4e} > 0$, enlarging output displacement leads to the following multi-objective optimization problem:

$$\begin{aligned}
 \min \quad & \omega(-|x_2|) + (1 - \omega)|x_4| \\
 \text{s.t.} \quad & t_{\min} \leq t_j \leq h \\
 & \sqrt{2 \left(\frac{l_j}{\theta_{hj}} \right)^2 (1 - \cos \theta_{hj})} \leq L_{n-\max} \\
 & \delta_{\min} \leq \frac{l_j}{t_j} \leq \delta_{\max} \\
 & 0 < \theta_{hj} < \pi \\
 & l_j > 0 \quad (j = A, B),
 \end{aligned}
 \tag{22}$$

where the range of weight ω is [0, 1]. The parameter t_{\min} denotes the lower limit of t , which depends on the fabrication ability. In the second constraint, the maximum length of nominal axis for the CALT flexure hinge $L_{n-\max}$, which influences the size of DAM, is set. Since the CALT flexure hinges are satisfied with Euler-Bernoulli beam assumption, the lower limit of $\frac{l_j}{t_j}$ should be set (such as

Table 1 Preset parameters of the optimal design example

h (mm)	L_2 (mm)	t_r (mm)	F_{in} (N)	δ_{\max}
6.00	10.00	1.50	10.00	10.00

Table 2 Initial value of the optimal design example

Group	l_A (mm)	t_A (mm)	θ_A	l_B (mm)	t_B (mm)	θ_B
1	5.50	0.60	$\pi/6$	5.50	0.60	$\pi/6$
2	3.50	0.50	$\pi/4$	5.50	0.60	$\pi/6$
3	4.50	0.45	$\pi/5$	4.50	0.45	$\pi/5$

Table 3 Pareto solutions of optimal problem (22)

ω	l_A (mm)	t_A (mm)	θ_A	l_B (mm)	t_B (mm)	θ_B
1.00	2.50	0.25	$\approx \pi$	2.50	0.25	≈ 0
0.50	2.50	0.25	$\approx \pi$	2.50	0.25	≈ 0
0.25	2.50	0.25	$\approx \pi$	2.43	0.25	≈ 0
0.20	2.50	0.25	$\approx \pi$	1.95	0.25	≈ 0
0.15	2.50	0.25	$\approx \pi$	1.69	0.25	$\approx \pi$
0.10	2.50	0.25	$\approx \pi$	1.28	0.25	$\approx \pi$
0.05	2.50	0.25	2.64	1.25	0.25	$\approx \pi$
0.02	3.99	0.80	≈ 0	6.26	1.25	$\approx \pi$

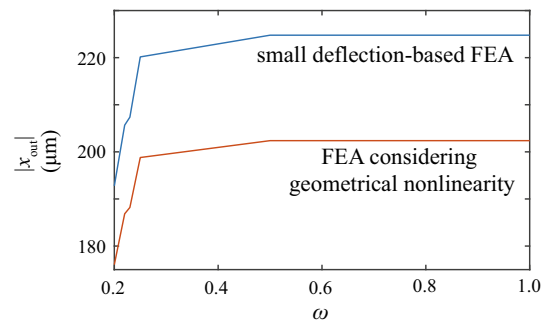


Fig. 4 $|x_{out}|$ v.s. ω (FEA results)

$\delta_{\min} = 5$). Considering the stress concentration and the fabrication ability, the upper limit of $\frac{l_j}{t_j}$ is set.

An optimal design example is given and the optimal result is determined from the Pareto solutions. The material is chosen as 7075-aluminum alloy, and other preset parameters are shown in Table 1. Three groups of initial value are listed in Table 2, in which the parameters are subject to the constraints in Eq. (22). The Matlab function “fmincon” is used to solve optimal problem (22), and the Pareto solutions are shown in Table 3. For different Pareto solutions, $|x_{out}|$ can be obtained by small deflection-based FEA, as shown in Fig. 4, which indicates that when $\omega = 1$, the maximum $|x_{out}|$ is obtained. Therefore, the Pareto solution corresponding to $\omega = 1$ is the optimal result. According to Fig. 4, even if geometrical nonlinearity is considered, the optimal dimensions will not be changed.

Table 4 Comparison between the theoretical results according to Eq. (5) and the small deflection-based static FEA results ($F_{ys} = 0$, $F_{xs} = 1$ N, $M_s = 0$)

θ_h	x_s (μm)		Error (%)
	Theoretical	FEA	
60°	17.300	16.053	7.71
80°	16.200	14.874	8.91
120°	13.400	12.109	10.66
140°	11.800	10.763	9.63
180°	8.600	7.648	12.45

Table 5 Comparison between the theoretical results according to Eq. (5) and the small deflection-based static FEA results ($F_{ys} = 1$ N, $F_{xs} = 0$, $M_s = 0$)

θ_h	x_s (μm)		Error (%)
	Theoretical	FEA	
60°	-2.300	-2.153	6.83
80°	-2.900	-2.678	8.29
120°	-3.600	-3.273	9.99
140°	-3.800	-3.487	8.98
180°	-3.600	-3.350	7.46

5 FEA verification and design validation

5.1 FEA verification of the deflection model for CALT flexure hinge

ANSYS workbench is used for the small deflection-based FEA verification. The material of beam ABCD is set as 7075-aluminum alloy (Young’s modulus 71 GPa, Poisson’s ratio 0.33). The parameters L , t and b are set as 3, 0.3 and 3 mm respectively. For different loads and θ_h , the comparison between the theoretical results according to Eq. (5) and the FEA results is shown in Tables 4 and 5.

Tables 4 and 5 show that the error of analytical model (5) is smaller than 12.50%. Therefore, the deflection model of CALT flexure hinge is effective. The shear effect ignored in the analytical model contributes to the error.

5.2 FEA verification of the optimal result

The small deflection-based FEA results of optimal results and initial groups are shown in Fig. 5a–d, which show that

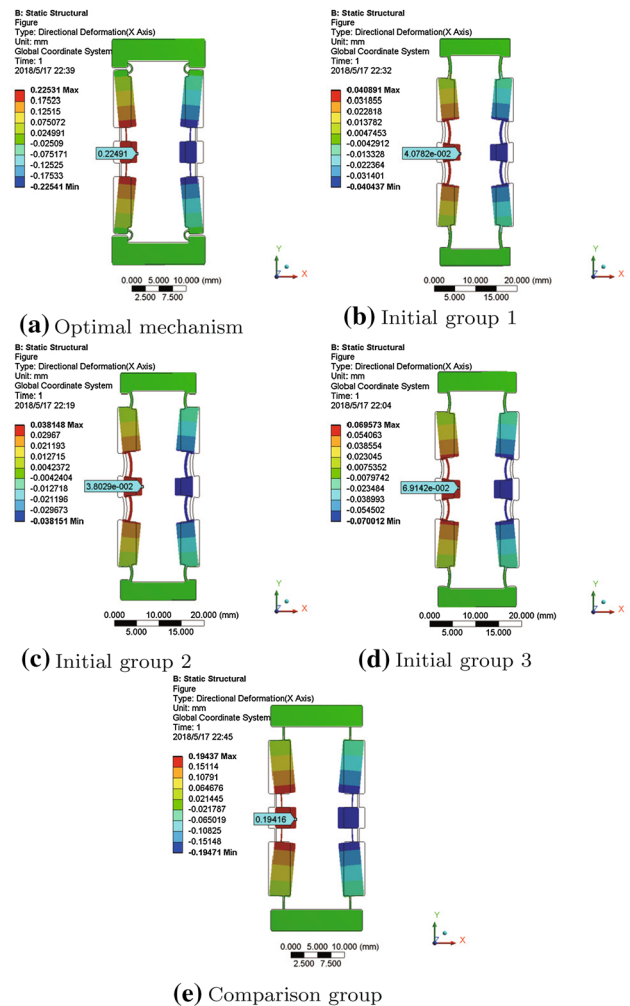


Fig. 5 Small deflection-based static FEA results of the optimal mechanism, the initial groups and the comparison group ($F_{in} = 10$ N)

the output displacement is obviously improved. Further, a comparison group is set. The difference between the optimal result and the comparison group is that the CALT flexure hinges ($\theta_h \approx \pi$) in the former are replaced by the straight-axis flexure hinges in the latter. The small deflection-based FEA result of comparison group is shown in Fig. 5e, which is considered as the bridge-type mechanism with the largest output displacement in the previous researches, but the output displacement of optimal result is larger than that of the comparison group by 15.84%.

5.3 Design validation

The optimal design results is further applied to construct a piezoelectric-driven microgripper for the design validation, as shown in Fig. 6a, in which the bidirectional symmetric input forces F_{in} are supplied by a piezoelectric stack actuator (Gu and Zhu 2013). To facilitate the mounting,

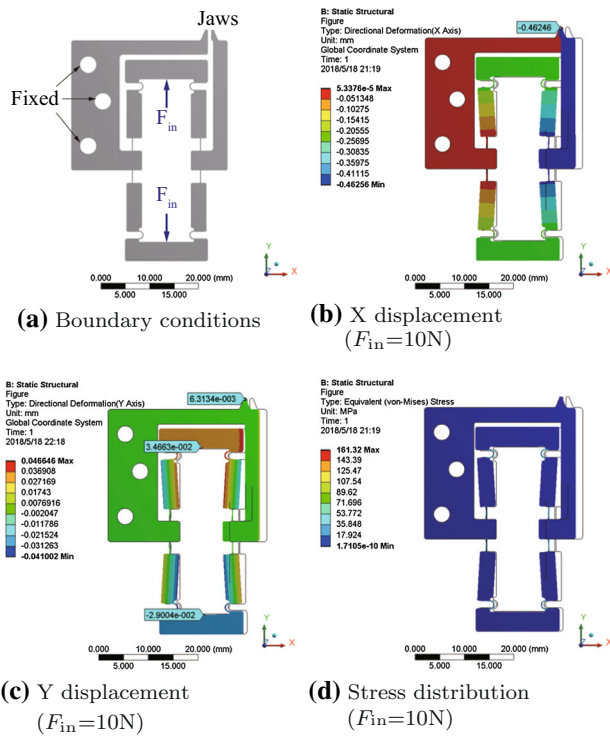


Fig. 6 Microgripper utilizing the optimal mechanism and the small deflection-based static FEA results ($F_{in} = 10\text{ N}$)

one of the output ports is fixed, leading to the left fixed jaw. The other output port is extended to form the right gripper arm with moving jaw.

Figures 5a and 6b indicate that, when an output port is fixed, the movements of both output ports are superimposed to the moving one. According to Fig. 6c, Y-axis parasitic movement exists at the moving jaw, which is because when an output port is fixed, the input displacements are different. Whereas the Y-axis parasitic movement at the moving jaw is only 1.37% of the X-axis grasping movement, verifying the parallel grasping movement. With the combination of Fig. 6b and c, the displacement amplification ratio of gripper is 14.64 in average. Therefore, grasping parallelly and enlarging the grasping stroke are obtained simultaneously. Figure 6d indicates that when $F_{in} = 10\text{ N}$, the maximum stress is 161.32 Mpa, which is far smaller than the yield stress of 7075-aluminum alloy, and the safety of microgripper is hence verified.

6 Conclusion

This paper designs, analyze and validate a bridge-type mechanism with circular-axis leaf-type (CALT) flexure hinges, which vary from typical straight-axis flexure hinges to typical curve-axis flexure hinges with the change of

radius angles. Through modeling the generalized displacements of CALT flexure hinge, the positive direction of its axis in the bridge-type mechanism is designed. The precise model of load relations for the CALT flexure hinges in the bridge-type DAM is established, and the multi-objective parametric optimization is further given. Small deflection-based static FEA results show that the error of nominal deflection model for CALT flexure hinge is smaller than 12.50%. The parametric optimization result is verified by FEA as well. Compared with the corresponding bridge-type mechanism with the largest output displacement in the traditional researches, the output displacement of optimal result is improved by 15.84%. The optimal design result is further applied to construct a piezoelectric-driven microgripper for the design validation, in which the parasitic movement at the jaw is only 1.37% of the grasping movement, and the displacement amplification ratio is 14.64 in average. Therefore, grasping parallelly and enlarging the output stroke are realized simultaneously.

Acknowledgements This research is supported by the National Natural Science Foundation of China (Grant 51705076), the Natural Science Foundation of Guangdong Province (Grant nos. 2016A030313481, 2015A030310181), the Science and Technology Planning Project of Guangdong Province (Grant no. 2015B010101015), the Scientific and Technological Innovation Special Funding of Foshan (Grant no. 2015AG10018), the High-Level Talent’s Research Funding of Foshan University (Grant no. Gg07092). The authors gratefully acknowledge these support agencies. The authors would like to thank to Ms. Yanshan Zhuang for her advice to the English writing.

References

Chen G (2014) Generalized equations for estimating stress concentration factors of various notch flexure hinges. *J Mech Des* 136(3):252–261

Chen W, Shi X, Chen W, Zhang J (2013) A two degree of freedom micro-gripper with grasping and rotating functions for optical fibers assembling. *Rev Sci Instrum* 84:115111

Chen W, Zhang X, Fatikow S (2017a) Design, modeling and test of a novel compliant orthogonal displacement amplification mechanism for the compact micro-grasping system. *Microsyst Technol* 23(7):2485–2498

Chen W, Zhang X, Li H, Wei J, Fatikow S (2017b) Nonlinear analysis and optimal design of a novel piezoelectric-driven compliant microgripper. *Mech Mach Theory* 118:32–52

Dong W, Chen F, Yang M, Du Z, Tang J, Zhang D (2017) Development of a high-efficient bridge-type mechanism based on negative stiffness. *Smart Mater Struct* 26(9):095053

Gu GY, Zhu LM (2013) Motion control of piezoceramic actuators with creep, hysteresis and vibration compensation. *Sens Actuators A Phys* 197(7):76–87

Ham YB, An BC, Trimzi MA, Lee GT, Park JH, Yun SN (2016) An experimental study on the displacement amplification mechanism driven by piezoelectric actuators for jet dispenser. *International conference on manipulation. Automation and robotics at small scales. IEEE, Paris*, pp 1–5

Howell LL (2001) *Compliant mechanisms*. Wiley, New York

- Kim JH, Kim SH, Kwak YK (2003) Development of a piezoelectric actuator using a three-dimensional bridge-type hinge mechanism. *Rev Sci Instrum* 74(5):2918–2924
- Kim JJ, Choi YM, Ahn D, Hwang B, Gweon DG, Jeong J (2012) A millimeter-range flexure-based nano-positioning stage using a self-guided displacement amplification mechanism. *Mech Mach Theory* 50(2):109–120
- Kozuka H, Arata J, Okuda K, Onaga A, Ohno M, Sano A, Fujimoto H (2013) A compliant-parallel mechanism with bio-inspired compliant joints for high precision assembly robot. In: *Procedia CIRP-Bio 2013*, vol 5, pp 175–178. Elsevier, Tokyo
- Lin R, Zhang X, Long X, Fatikow S (2013) Hybrid flexure hinges. *Rev Sci Instrum* 84(8):085004
- Liu M, Zhang X, Fatikow S (2017a) Design and analysis of a multi-notched flexure hinge for compliant mechanisms. *Precis Eng* 48:292–304
- Liu Y, Zhang Y, Xu Q (2017b) Design and control of a novel compliant constant-force gripper based on buckled fixed-guided beams. *IEEE/ASME Trans Mechatron* 22(1):476–486
- Lobontiu N, Cullin M (2013) In-plane elastic response of two-segment circular-axis symmetric notch flexure hinges: the right circular design. *Precis Eng* 37(3):542–555
- Lobontiu N, Garcia E (2003) Analytical model of displacement amplification and stiffness optimization for a class of flexure-based compliant mechanisms. *Comput Struct* 81(32):2797–2810
- Ma F, Chen G (2015) Modeling large planar deflections of flexible beams in compliant mechanisms using chained beam-constraint-model. *J Mech Robot* 8(2):021018
- Mottard P, Stamant Y (2009) Analysis of flexural hinge orientation for amplified piezo-driven actuators. *Smart Mater Struct* 18(3):035005
- Piriyanont B, Fowler AG, Moheimani SOR (2015) Force-controlled mems rotary microgripper. *IEEE/ASME J Microelectromech Syst* 24(4):1164–1172
- Pokines BJ, Garcia E (1998) A smart material microamplification mechanism fabricated using liga. *Smart Mater Struct* 7(1):105–112
- Sun X, Chen W, Fatikow S, Tian Y, Zhou R, Zhang J, Mikczinski M (2015) A novel piezo-driven microgripper with a large jaw displacement. *Microsyst Technol* 21(4):931–942
- Verotti M, Crescenzi R, Balucani M, Belfiore NP (2015) MEMS-based conjugate surfaces flexure hinge. *J Mech Des* 137(1):012301
- Wang N, Liang X, Zhang X (2015) Stiffness analysis of corrugated flexure beam used in compliant mechanisms. *Chin J Mech Eng* 28(4):776–784
- Wei H, Shirinzadeh B, Li W, Clark L, Pinskiar J, Wang Y, Wei H, Shirinzadeh B, Li W, Clark L (2017) Development of piezo-driven compliant bridge mechanisms: general analytical equations and optimization of displacement amplification. *Micromachines* 8(8):238
- Xing Q (2015) Design of asymmetric flexible micro-gripper mechanism based on flexure hinges. *Adv Mech Eng* 7(6):1–8
- Xu Q, Li Y (2011) Analytical modeling, optimization and testing of a compound bridge-type compliant displacement amplifier. *Mech Mach Theory* 46(2):183–200
- Yong YK, Lu TF, Handley DC (2008) Review of circular flexure hinge design equations and derivation of empirical formulations. *Precis Eng* 32(2):63–70

Publisher's Note Springer Nature remains neutral with regard to jurisdictional claims in published maps and institutional affiliations.